

Theoretical Insights into the Inhibition Performance of Three Neonicotine Derivatives as Novel Type of Inhibitors on Carbon Steel

Yun Wang¹, Zhen Wang², Lei Zhang^{1,*} and Minxu Lu¹

¹University of Science and Technology Beijing, Beijing, 100083, China

²Nanjing University of Aeronautics and Astronautics, Nanjing, 211106, China

*Corresponding Author: Lei Zhang. Email: zhanglei@ustb.edu.cn

Received: 10 December 2019; Accepted: 18 February 2020

Abstract: The adsorption process of new nicotinic derivatives on Fe (110) surface and diffusion of corrosive particles in inhibition film were studied by quantum chemistry and molecular dynamics simulation, and inhibition mechanism of inhibitor was discussed. The results indicated that the main active sites of three inhibitors are located in N atoms on the five membered ring. The inhibitor YM-1 has the strongest activity of electrophilic reaction, and the adsorption process of inhibitor molecules is polycentric chemisorption. The adsorption energy for inhibitors followed the order of YM-1 > YM-2 > YM-3. The adsorption film YM-1 more effectively impedes the diffusion and migration of the corrosive particles, and also has the best inhibitory effect on Cl⁻. In addition, the bond energy of chemical bond formed between inhibitor and Fe atom increases as the increase of temperature. The interaction between corrosive particles and inhibitors is dominated by Van der Waals force.

Keywords: Molecular dynamics; bond energy; adsorption; FFV; nucleophilic ability

1 Introduction

The corrosion of carbon steel has become a serious problem that can not be ignored in the process of oil and gas exploitation, which seriously troubled the development of oil and gas industry at home and abroad [1]. A large number of pipelines in oilfield will be corroded, perforated and even invalidated due to CO₂ corrosion [2–5]. In addition, Cl⁻ can not be neglected in corrosion of steel because the passive films on metal surface are easily destroyed by this anion [6–9]. At the same pH value, the total acidity of CO₂ is higher than that of hydrochloric acid, thus the corrosion of CO₂ water solution is stronger. For this reason, corrosion inhibitor containing N, S, P and O heteroatoms is widely used in oil and gas fields, which can be adsorbed on the steel surface to slow down the corrosion rate of metal [10–13]. Many kinds of corrosion inhibitors for carbon steel corrosion had been experimentally investigate, while traditional experimental measurement has a high cost, long time and even big error [14–17]. Recently, quantum chemical calculation and molecular dynamics simulation as effective method have been used to study the effect of organic inhibitors on metal surface. Kaya et al. [18] investigated the adsorption and corrosion inhibition properties of three piperidine derivatives on Fe (110), Fe (100) and Fe (111) surfaces by

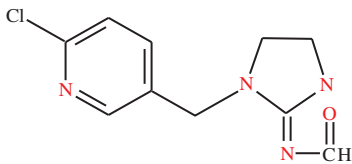
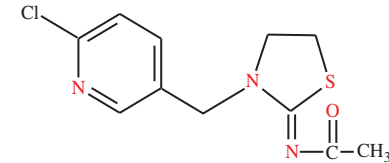
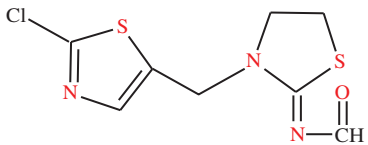


This work is licensed under a Creative Commons Attribution 4.0 International License, which permits unrestricted use, distribution, and reproduction in any medium, provided the original work is properly cited.

performing quantum chemical calculations and molecular dynamics simulations, the most effective inhibitor among them is FMPPDBS according to the binding energies. Shahraki et al. [19] studied the inhibition efficiencies of three amine derivatives on corrosion of carbon steel using the DFT method and molecular dynamic simulation in aqueous phase. The results reveal that pentaethyl-enehexamine as an inhibitor has the highest tendency to adsorb strongly onto the metal surface, and interaction energy values of the three inhibitor compounds with the Fe (110) surface obey the order III > II > I. Xie et al. [20] had adopted molecular dynamics simulation method to investigate the absorption behavior, inhibition mechanisms of 3,5-dibromo salicylaldehyde Schiff's base on Fe (1 0 0) surface in aqueous solution and the diffusion behavior of H_3O^+ , Cl^- and H_2O in inhibitor films. The results demonstrated that the absorption manner is a multi-center chemical adsorption for three inhibitor films. However, some inhibitors for metal corrosion are toxic, not easy to bio-degrade and also not friendly to the environment. The development of green inhibitors is a prospective trend for inhibiting the corrosion of metals.

In this study, the effect of H_3O^+ , HCO_3^- and Cl^- on corrosion of steel and inhibition mechanism of nicotine derivatives as a new kind of green inhibitor (Tab. 1), 1-(6-Chloropyridin-3-ylmethyl)-2-formyliminoimidazolidine (YM-1), 3-(2-Chloro-1,3-thiazol-5-ylmethyl)-2-formylimino-1,3-thiazolidine (YM-2), 3-(6-Chloropyridin-3-ylmethyl)-2-acetylimino-1,3-thiazolidine (YM-3), were investigated by quantum chemical and molecular dynamics simulation. The adsorption behavior of three corrosion inhibitors on the metal surface and the diffusion of corrosive particles in corrosion inhibitor film were also discussed.

Table 1: Molecular structures for three kinds of nicotine derivatives as inhibitors

Inhibitor	Name	Structure
YM-1	1-(6-Chloropyridin-3-ylmethyl)-2-formyliminoimidazolidine	
YM-2	3-(2-Chloro-1,3-thiazol-5-ylmethyl)-2-formylimino-1,3-thiazolidine	
YM-3	3-(6-Chloropyridin-3-ylmethyl)-2-acetylimino-1,3-thiazolidine	

2 Computational Methods

2.1 Quantum Chemical Calculation

All quantum chemical calculations are performed using Density Functional Theory (DFT), which is certainly the most widely used methodology that can provide a very useful tool for understanding molecular chemical reactivity and describing the behaviour of atoms in molecules.

During DFT calculation, the generalized gradient approximation (GGA) method with DNP basis set, in the form of the Perdew-Burke-Ernzerhof approximation, was used to calculate the exchange-correlation energy without any symmetry and spin constraints [21,22]. DFT-D correction was used for dispersion corrections. The parameter criteria for the convergence thresholds of energy change, maximum force and

maximum displacement are 1.0×10^{-5} Ha, $0.002 \text{ Ha}/\text{\AA}$ and $5.0 \times 10^{-3} \text{\AA}$, respectively [23]. The global orbital cutoff is 4.6\AA , and the self-consistent field tolerance is 1.0×10^{-6} Ha. This basis set provided accurate geometry and electronic properties for a wide range of organic compounds. The global parameters, frontier orbital distribution, chemical potential of the molecule (χ), hardness (η), soft (σ), electrophilicity index (ω) and nucleophilicity (ε), are used for the analysis of molecular reaction activity and selectivity. Besides, molecular electrostatic potential (MEP) and frontier molecular orbitals were determined at B3LYP/6-31G* level of theory. The values of the highest occupied orbital energy E_{HOMO} and the lowest unoccupied orbital energy E_{LUMO} are obtained. Before the calculation, some structural parameters of H_2O and crystal Fe are calculated based on these parameters (Fig. 1). The calculated values of the O-H bond length and H-O-H bond angle of H_2O are 0.976 nm , 104.5° respectively, and the lattice constant of Fe is 0.287 nm , which are in good agreement with the experimental values [24].

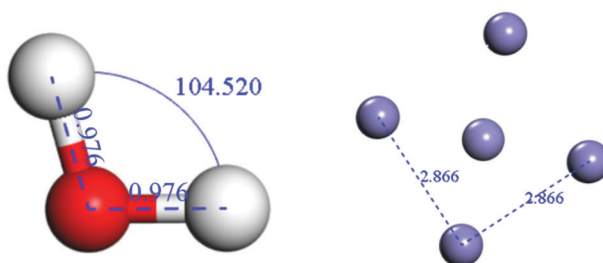


Figure 1: Structural parameters of H_2O and crystal Fe

According to Hartree-Fock theorem, the ionization potential (I) and the electron affinity (A) are given as follow:

$$I = -E_{\text{HOMO}} \quad (1)$$

$$A = -E_{\text{LUMO}} \quad (2)$$

As a result of this theorem, chemical potential and chemical hardness can be expressed as:

$$\chi = \frac{I + A}{2} \quad (3)$$

$$\eta = \frac{I - A}{2} \quad (4)$$

The global softness is defined as the inverse of the global hardness and this quantity is given as [25,26]:

$$\sigma = \frac{1}{\eta} \quad (5)$$

The global electrophilicity index (ω) is given below in Eq. (6). From the light of this index, electrophilic power of a chemical compounds is associated with its electronegativity and chemical hardness. Nucleophilicity (ε) is the inverse of the electrophilicity as is given below in Eq. (7) [27]:

$$\omega = \frac{\mu^2}{2\eta} = \frac{\chi^2}{2\eta} \quad (6)$$

$$\varepsilon = \frac{1}{\omega} \quad (7)$$

2.2 Molecular Dynamics Simulation

Molecular dynamics (MD) simulation is an important computer simulation method applied to various systems for solving many body problems at the atomic and molecular levels, which is used to study the diffusion of corrosive particles in the corrosion inhibition film and interaction between inhibitor and the concerned metal surfaces. Forcite module was used to determine inhibitor molecule conformers applying the force field COMPASS in order to perform energy minimization and MD calculation processes [28]. The obtained conformers were pre-geometrized using the algorithm named smart. The electrostatic interaction and the Van der Waals forces were calculated atom by atom.

Fe (110) was selected due to the most stable surface compared with other Fe surfaces and more active sites on the surface [29]. Corrosive particles (HCO_3^- , Cl^- , H_3O^+) and 100 organic inhibitor molecules were built in an amorphous cubic cell (Fig. 2). Fe (110) surface model with 5-layer atom, corrosive medium and 20 Å vacuum layer is used to study the adsorption of organic inhibitor molecules on Fe surface, the model size is $39.72 \times 39.72 \times 69.54 \text{ \AA}^3$. The structure of MD simulation is optimized by COMPASS force field to ensure the accuracy of calculation results, and then the cell was performed to dynamic calculation [30–32]. After equilibrium, the average value of the system density was used as the density of the corrosion inhibitor film in the calculation system. Then, NVT (constant molecule numbers, volume and temperature) ensemble method was carried out at 303 K to reach molecular structures under an equilibrium state, and the time step for the MD simulation is 0.1 fs with a period of 500 ps, followed by simulating in NVE ensemble for 1000 ps [33]. In these simulations, the temperature was controlled by Andersen thermostat, the initial velocity of each molecule is randomly generated by the distribution of Maxwell-Boltzmann; the velocity verlet's algorithm is used to solve the Newton equation of motion on the basis of the assumption that the periodic boundary conditions and the time average are equivalent to the ensemble average, the values of Van der Waals and Coulomb interaction were calculated by charge group method [34,35]. The cut-off radius is 1.5 nm, the intermolecular interaction beyond the cut-off distance is corrected by the average density approximation method.

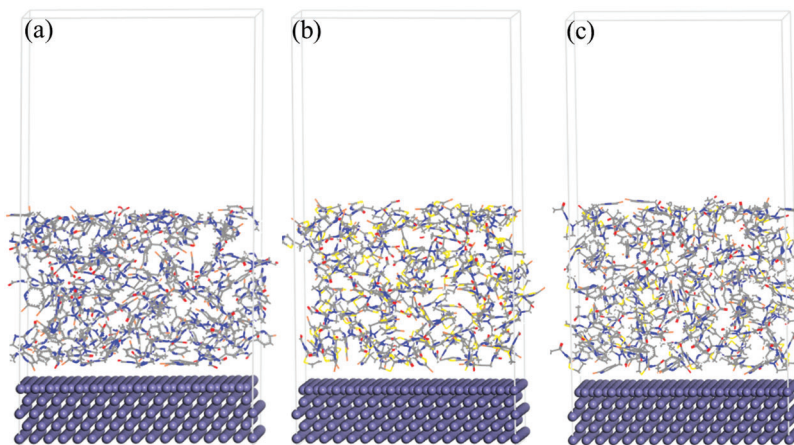


Figure 2: Models of corrosive particles diffusion in corrosion inhibitor membrane. (a) YM-1; (b) YM-2; (c) YM-3

The interaction energy between the metal and the inhibitors were calculated according to the following equation [36]:

$$E_{\text{adsorption}} = (E_{\text{molecule}} + E_{\text{surface}}) - E_{\text{total}} \quad (8)$$

where, $E_{\text{adsorption}}$ is the adsorption energy, E_{molecule} is the energy of free molecules; E_{surface} is the energy of the metal surface that the molecule is not adsorbed; E_{total} is the total energy of a molecule and a metal surface system.

The negative magnitude of interaction energy gives the values of binding energy:

$$E_{\text{blinding}} = -E_{\text{adsorption}} \quad (9)$$

3 Results and Discussion

3.1 Electronic Structure Analysis

Quantum chemical calculation was carried out to discuss the frontier orbital distribution of inhibitor molecules, the results are as shown in Fig. 3. For inhibitor YM-1, the HOMO orbit delocalization is at the sulfonic group in the end of chain, and the charge density of HOMO is concentrated around the S atom; the HOMO orbit delocalization is at the sulfonic group. This distribution means that the five membered ring containing N atom will be adsorbed preferentially when adsorption occurs, which is beneficial for the empty d orbital of metal surface to accepting electrons provided by inhibitors to form coordination bonds, on the contrary, inhibitor molecules can also receive electrons and form feedback bonds. Thus, it would lead to the stable adsorption of inhibitor on the surface of metal.

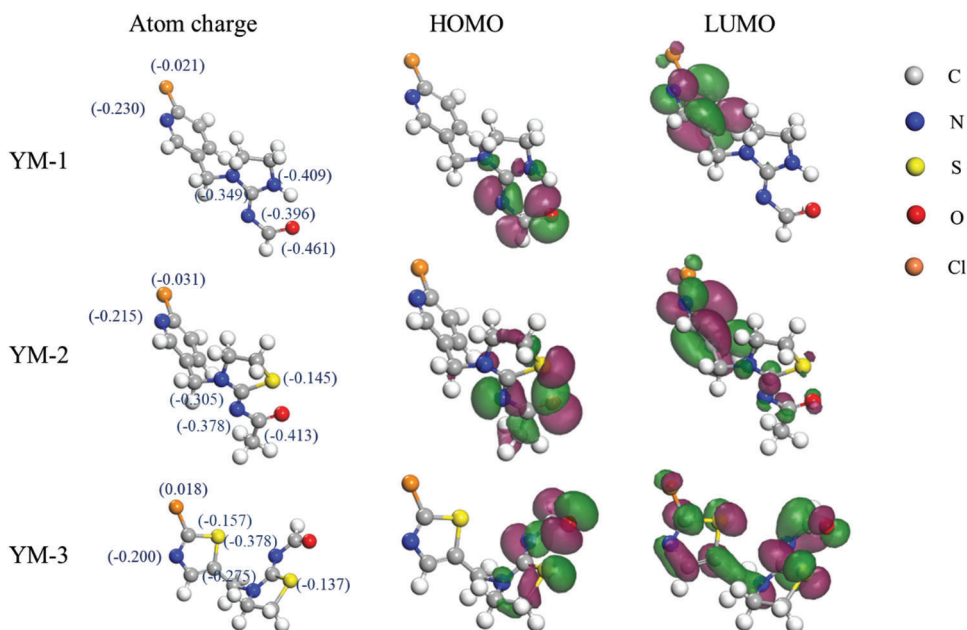


Figure 3: Frontier orbital energy distribution of frontier orbitals of inhibitor molecules

The calculated results of the quantitative parameters of the five kinds of inhibitors are shown in Tab. 2. Based on the quantum chemistry calculation of organic corrosion inhibitors, the calculated values of E_{HOMO} are $\text{YM-1} > \text{YM-2} > \text{YM-3}$. E_{HOMO} is a dimension of ability that molecular donates electrons. According to DFT theory, the greater the energy of the highest occupied molecular orbital (E_{HOMO}), the easier the corrosion inhibitor molecule donates electrons to unoccupied d orbital of the metal. In others words, inhibitor molecule that has lower value of E_{HOMO} is not easy to be adsorbed with the interface. Hence, YM-1 can easily contribute to the pair electrons on the N, S, O heteroatom and form coordinate-covalent bonds with the 3D hollow orbits in Fe atoms, showing more stronger nucleophilic ability.

Moreover, E_{LUMO} is a dimension of ability accepted electrons. The lower the energy of the lowest unoccupied molecular orbital (E_{LUMO}), more easily the corrosion inhibitor molecule receives electron from d orbital of the metal. It can be obtained from Tab. 2 the calculated values of E_{LUMO} are $\text{YM-3} > \text{YM-2} > \text{YM-1}$.

Table 2: Molecular properties of three inhibitors calculated with DFT method

Inhibitors	E_{HOMO} (eV)	E_{LUMO} (eV)	ΔE (eV)	χ (eV)	η (eV)	ω (eV)	ε (eV ⁻¹)	σ (eV ⁻¹)
YM-1	-5.43	-3.71	1.72	4.57	0.86	12.15	0.08	1.16
YM-2	-6.08	-2.59	3.49	4.33	1.75	5.37	0.18	0.57
YM-3	-6.09	-2.54	3.55	4.32	1.77	5.26	0.19	0.56

The energy gap values of inhibitor, ΔE ($\Delta E = (E_{\text{LUMO}} - E_{\text{HOMO}})$), increases in the order of YM-1, YM-2 and YM-3. It is generally believed that the energy gap is an important indicator of molecular stability. The ΔE is smaller, the organic molecules are more easily bound to Fe atoms on the metal surface through coordination bonds. Among the three inhibitors, ΔE value of YM-1 is the smallest, which indicates that YM-1 has higher activity and can form film on metal surface quickly. In addition, the chemical hardness (η) of the inhibitor YM-1 is the smallest, the chemical softness (σ), the absolute values of the chemical potential (χ) and the electrophilicity index (ω) are the largest. The results indicate that YM-1 has the strongest electrophilic reaction activity and is easy to lose the electrons. Therefore, the inhibitor YM-1 should have the best corrosion inhibition performance, which is consistent with the conclusion obtained from the above orbital energy difference.

3.2 Adsorption and Bond Length of Inhibitor Molecule on Fe (110) Surface

In the mixed solution containing HCO_3^- and Cl^- ions, the adsorption behaviour of three new nicotinic molecules on Fe (110) surface was studied by molecular dynamics simulation, and the equilibrium adsorption configuration of molecules was shown in Fig. 4.

It can be seen from Fig. 4 that the adsorption state of three kinds of inhibitor molecules on Fe (110) crystal plane is horizontal adsorption, which indicates that the -N=, -C=N- and -S- functional groups have strong interaction on the metal interface. From the equilibrium adsorption configuration of molecules, it can be seen that the adsorption configuration of YM-1 molecules is more obvious. In the process of adsorption, a more compact adsorption film can be formed to prevent the invasion of corrosive medium.

The bond length between a molecule and metal Fe atom is an important parameter to measure the adsorption intensity, and can also be used to determine the type of interaction. In general, the bond length is within the range of 1~3.5 Å when chemical adsorption occurs, while the bond length of physical adsorption is more than 3.5. The radial distribution function (RDF) is an effective method to measure the length of the atomic bond, and the horizontal ordinate value of the first peak in the curve is marked as the bond length. The RDF results of the N and S atoms of the three inhibitors are shown in Fig. 4. The bond length of the iron atom with N and S is less than 3.5, which indicates that there exists chemical adsorption between corrosion inhibitor molecules and Fe (110) surface. As is shown in Fig. 4, the equilibrium adsorption structures of YM-2 and YM-3 molecule have varying degrees of torsion. In addition, by comparing the bond length of the chemical bond between the three inhibitors and the Fe atoms on the metal surface, the bond length of the inhibitor YM-1 is shorter, which indicates that the corrosion inhibition film formed by the inhibitor molecule YM-1 on the surface of the metal is more stable.

The adsorption energy of the inhibitors interacted with Fe (110) crystal surface in the solution are listed in Tab. 3. It can be seen from Tab. 3 that the absolute values of the adsorption energy are 546.57 kJ mol⁻¹, 533.05 kJ mol⁻¹, 132.52 kJ mol⁻¹, successively, the adsorption energy of three new nicotinic derivatives in solution increases in sequence, which indicates that the adhesion between YM-1 and metal surface is stronger, and the stability of adsorption film is also better. Two N atoms with lone pair electrons on the five membered ring and Fe atoms may lead to multiple adsorption center. In addition, the C=N double

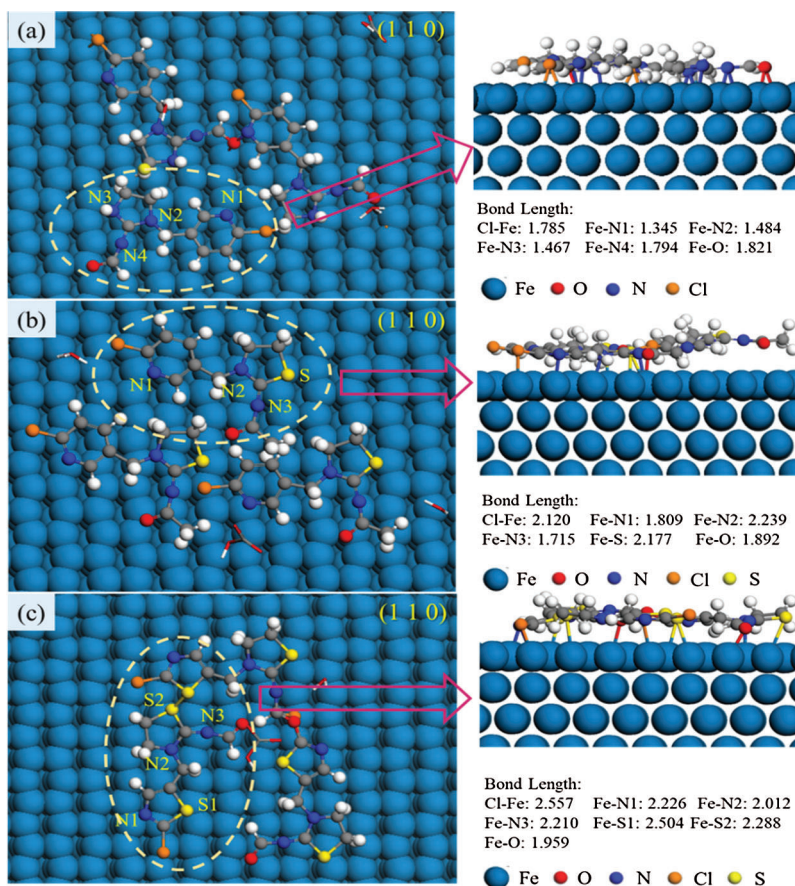


Figure 4: Equilibrium adsorption configuration of inhibitor molecules and bond length (a): YM-1, (b): YM-2, (c): YM-3

Table 3: The adsorption energy on Fe (110) surface for three inhibitor molecules

Inhibitors	$E_{\text{total}} \times 10^{-6}$ (kJ mol ⁻¹)	$E_{\text{surface}} \times 10^{-6}$ (kJ mol ⁻¹)	$E_{\text{initiation}}$ (kJ mol ⁻¹)	$E_{\text{interaction}}$ (kJ mol ⁻¹)	E_{binding} (kJ mol ⁻¹)
YM-1	9.5909	9.5919	-414.86	-546.57	546.57
YM-2	9.5912	9.5920	-281.74	-533.05	533.05
YM-3	9.5906	9.5915	-832.17	-132.52	132.52

bond in the inhibitor molecule can also form the π -d bond with the metal, so it has good adsorption capacity. The introduction of the group contained N, Cl atoms with unshared electrons on the N atom of C-N and the carbonyl group on the N atoms of the C=N double bond can increase the number of adsorption center, and further change the density of the bond electron cloud in the inhibitor molecule. It can change the adsorption capacity of the central atom through the inductive effects and enhance the chemical adsorption with the iron atom. Moreover, the hydrophobic group in the molecule increases the hydrophobicity of the inhibitor, which is beneficial to the formation of the adsorption film, and increases the density of the adsorption film, thus improving the corrosion inhibition performance. The adsorption energy of the inhibitors is negative, and the adsorption effect is belongs to exothermic process.

In addition, the lone pair electrons existed in the central atom N, O and S of inhibitors may react with H^+ ionized by corrosive solution, forming cations. The cations will be adsorbed on the surface of the metal Fe by electrostatic action, thus positive charge would be carried on metal. As a result, it hinders the contact of H^+ from metal interface, and the activation energy of the hydrogen ion discharge is increased, the rate of corrosion is greatly slowed down.

3.3 Diffusion of Different Corrosive Particles in Corrosion Inhibition Film

The diffusion coefficient of the corrosive particles in the inhibitor film was easily obtained using the Einstein relationship:

$$MSD = \langle |R_i(t) - R_i(0)|^2 \rangle \quad (10)$$

$$D = \frac{1}{6N} \lim_{t \rightarrow \infty} \frac{d}{dt} \sum_{i=1}^N \langle |R_i(t) - R_i(0)|^2 \rangle = a/6 \quad (11)$$

where, N is the total number of molecule or particles in the system, $R_i(t)$ and $R_i(0)$ represent the location of inhibitor molecule or particle in t and initial time. A represents the curve slope of mean square displacement (MSD) to time. D is the diffusion coefficient.

Fig. 5 shows diffusion coefficients of corrosive particles and fractional free volume (FFV) in corrosion inhibitor films at 303 K. The diffusion coefficient can quantitatively evaluate the diffusion capacity of the corrosive medium particles in the corrosion inhibitor film. The smaller the diffusion coefficient of the corrosive medium particles is, the weaker the diffusion and migration ability of the particles is, which indicates that the corrosion inhibition performance of the corrosion inhibitor is better. It is shown from Fig. 5 that the diffusion coefficient of H_2O in the inhibition film decreased greatly by comparing with the result ($3.379 \times 10^{-9} \text{ m}^2 \text{ s}^{-1}$) in pure water [37]. The diffusion coefficients of three kinds of corrosive particles in different corrosion inhibition films has a certain difference. By analysing, the inhibition ability of different corrosion inhibitor molecular films to the diffusion of different corrosive medium particles is different. The diffusion coefficient of Cl^- , H_3O^+ and HCO_3^- are smaller in YM-1 inhibition film than that of YM-2 and YM-3, which indicates that YM-1 inhibition film effectively hinders the moving speed of corrosive particles. In addition, a hydrogen bond may be formed through the carbonyl group in the inhibitor molecule, which can improve the self-stability of the inhibitor film. The polarity of aldehydes

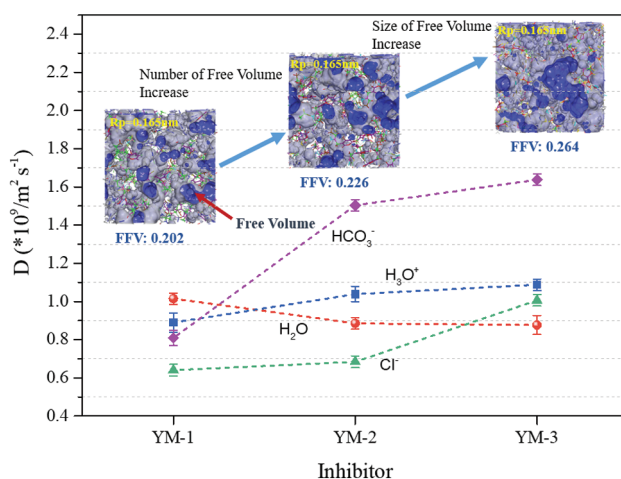


Figure 5: Diffusion coefficients of H_2O (a), H_3O^+ (b), HCO_3^- (c), Cl^- (d) corrosive particles in three corrosion inhibition films

(-CHO) is greater than that of ketones (-CO-). The inhibition film wrapped up the corrosive particles tightly. In addition, there is intermolecular hydrogen bond formed by imino (-NH-). It can effectively improve the resistance of the corrosion reaction and slow down the rate of corrosion.

Fractional free volume (FFV) can measure the compactness of membrane system [38–40]. To a certain extent, it reflects the difficulty degree of particles diffusing in a membrane, and the value is equal to the percentage of free volume in the membrane to total volume. The van der Waals radius should be obtained before calculating the free volume of particles in the membrane. The free volume of the system is calculated by using the Atom Volume & Surface. In the hard sphere probe model, the kinetic radius of CO₂ molecules is 0.165 nm [41]. The free volume spatial distribution of different inhibitors is shown in Fig. 5, it can be seen clearly that the value of free volume tends to increase in three inhibitor systems. In general, the greater the free volume fraction (FFV) of a polymer is, the greater the diffusion coefficient is [42], which is in agreement with that of the results of diffusion coefficient. The results indicate that the volume that gas molecules can reach in the inhibition film system decreases, slowing down the rate of CO₂ corrosion occurred on the surface of carbon steel due to inhibition film that hinders the contact between metal and corrosion solution. Therefore, the inhibition effect of inhibitor YM-1 is obviously better than that of others.

3.4 Effect of Temperature on the Diffusion of Corrosive Particles Corrosion Inhibition Film

The curves of energy in the inhibitor film YM-1 at different temperatures were shown in Fig. 6. As can be seen from Fig. 6, the interaction energy between charged particles and corrosion inhibitors can be far more than that of water molecule. As the temperature rises, the diffusion coefficient of the corrosive particles decreases gradually. It indicates that the binding ability of corrosion inhibitor to corrosive particles is enhanced, and increasing the density of the film.

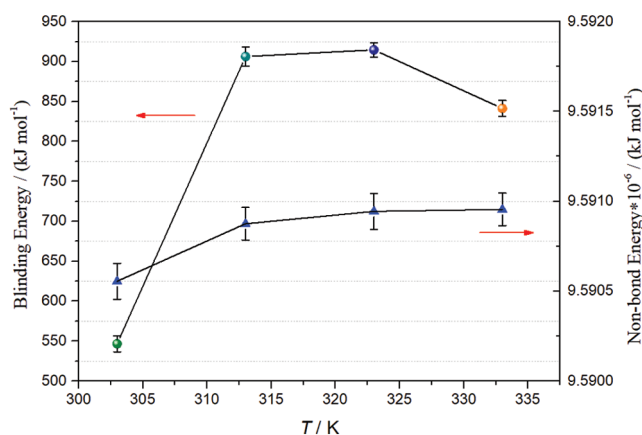


Figure 6: Binding energy and non-bond energy in the inhibitor film YM-1 at different temperatures

As the temperature rises from 303 to 333 K, the bond energy of chemical bond formed between the corrosion inhibitor and the metal atom rise sharply. When the temperature is up to 323 K, the maximum adsorption energy is 914.62 kJ mol⁻¹. It may be that the corrosion inhibitor molecules move faster to the metal surface with rising of temperature. The water molecules located on the metal surface are squeezed out by inhibitor molecules, the corrosion inhibitor molecules quickly occupy the activation site and adsorb on the surface. Macromolecules replace small molecules on the surface, which makes the density of the surface inhibition film increase and accelerates the diffusion of water molecules in the bulk solution.

Table 4: Coulomb interaction energies (E_{Coulomb}) and van der Waals interaction energies (E_{vdW}) in corrosion inhibitor film YM-1 at different temperatures

T (K)	$E_{\text{vdW}} \times 10^{-4}$ (kJ mol ⁻¹)	$E_{\text{Coulomb}} \times 10^{-3}$ (kJ mol ⁻¹)	$E_{\text{non-bond}} \times 10^{-4}$ (kJ mol ⁻¹)
303	-2.005	-8.199	-2.825
313	-2.144	-8.186	-2.963
323	-2.181	-8.307	-3.012
333	-2.180	-8.433	-3.023

From the point of molecular dynamics simulation, the interaction between the corrosion inhibitor film and the corrosive particle includes Coulomb force and Van der Waals' force. The energy of Coulomb interaction and Van der Waals' interaction between the corrosion inhibitor film and the corrosive particles are listed in [Tab. 4](#).

From the data of [Tab. 4](#), it is known that the interaction between corrosive particles and corrosion inhibitors is dominated by Van der Waals force. The interaction energy between charged particles and corrosion inhibitors can be far more than that of water molecule, which is attributed to the small diffusion coefficient of charged particles. As the temperature rises, the diffusion coefficient of the corrosive particles decreases gradually, and the binding energy increases first and then decreases.

Thus, it indicates that both density and stability of the inhibition film are enhanced, the inhibition performance of the corrosion inhibition film blocking the diffusion of the charged particles to the metal surface is stronger, effectively hindering the accumulation of corrosive particles at the metal/solution interface, and the rate of corrosion reaction is reduced.

4 Inhibition Mechanism

Based on the previous simulation results, the corrosion inhibition mechanism of the new nicotine derivatives on the surface of carbon steel can be explicated as shown in [Fig. 7](#).

When the organic corrosion inhibitor is added into corrosive medium, the water molecules adsorbed on the surface of the metal Fe are replaced by the inhibitors molecule. Due to the active dissolution of iron, Fe could be oxidized to Fe^{2+} , and ultimately Fe^{2+} will interact with the inhibitor molecule adsorbed on the iron surface ($\text{Inh}_{(\text{ads})}$) through chemical bond, forming the Fe(II)-Inh complex adsorbed on the iron surface.



Two N atoms with lone pair electrons on the five membered ring will form multiple center of adsorption with Fe atoms, the C=N bond in the molecule can also form a π -d bond with the metal, it possesses a good adsorption capacity. The group of N atoms with unshared electron pairs is introduced into the C atom of C-N in the five membered ring, which can increase the adsorption center and further improve the corrosion inhibition performance of the corrosion inhibitor. The carbonyl group containing O atoms is added to the N atoms of C=N bond, increasing the electron cloud density in the five membered ring, which can not only change the adsorption capacity of the central atoms by the induction effect and enhance the chemical adsorption with the iron atoms, but also the hydrophobic groups in the molecules increase the

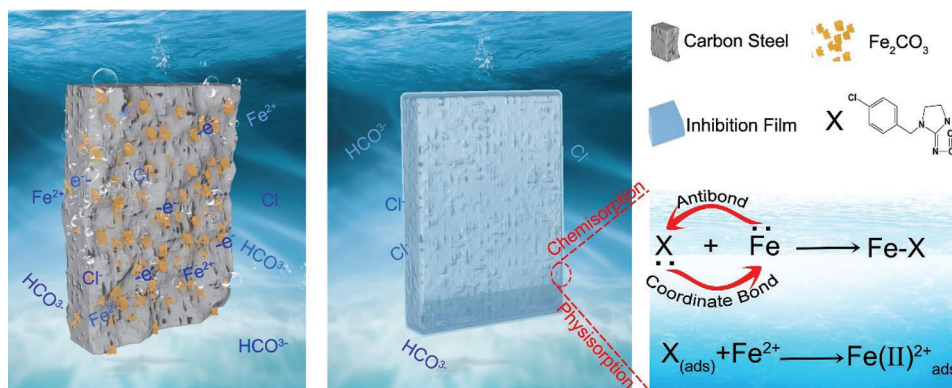


Figure 7: Corrosion and inhibition of carbon steel

hydrophobicity of the inhibitors. Thus, it is propitious to the formation of the adsorption film, increase the density of the adsorption film and also improve the corrosion inhibition performance.

5 Conclusions

In this work, the effect of H_3O^+ , HCO_3^- and Cl^- corrosive particles on Fe (110) surface and inhibition mechanism of YM-1, YM-2 and YM-3 as corrosion inhibitors were investigated by quantum chemical and molecular dynamics simulation methods.

1. The geometric structure, frontier orbital energy and orbital distribution, and the global parameters of three kinds of corrosion inhibitors were calculated through quantum chemical calculation. The three inhibitors have similar reactivity sites, and the main active sites are located in the N atoms on the five membered ring. By contrast, the inhibitor YM-1 has the strongest activity of electrophilic reaction, indicating that it has the best corrosion inhibition performance.
2. The mean square displacement curves of the corrosive particles H_2O , Cl^- , HCO_3^- and H_3O^+ in three kinds of corrosion inhibitors show that YM-1 has a strong inhibition effect on Cl^- anions. For H_3O^+ cation, the diffusion and migration ability in the YM-1 molecular adsorption film is relatively weak. The diffusion coefficient of corrosive particles H_2O , Cl^- , HCO_3^- and H_3O^+ in three kinds of corrosion inhibitor film and water molecular indicates that corrosion inhibitor YM-1 has strong inhibition ability to effectively controls the diffusion and migration of corrosive particles, and showing good corrosion inhibition performance. In addition, the diffusion coefficient of the corrosive particles decreases gradually with the increase of temperature, the binding ability of corrosion inhibitor film to corrosive particles is enhanced, and increasing the density of the film.
3. With the increase of temperature, the bond energy of chemical bond formed between the corrosion inhibitor and the metal atom rise. It may be that the corrosion inhibitor molecules move faster to the metal surface, and the water molecules located on the metal surface are squeezed out by inhibitor molecules, the corrosion inhibitor molecules quickly occupy the activation site and adsorb on the surface. In addition, the interaction between corrosive particles and corrosion inhibitors is dominated by Van der Waals force.

Acknowledgement: The authors thank the postgraduate students for their kind help. The authors also sincerely thank the anonymous reviewers for their constructive suggestions.

Funding Statement: This work was supported by the National Key R & D Program of China under Grant [No. 2017YFC0805800-02].

Conflicts of Interest: The authors declare that they have no conflicts of interest to report regarding the present study.

References

1. Chen, Z. Y., Huang, L., Zhang, G. A., Qiu, Y. B., Guo, X. P. (2012). Benzotriazole as a volatile corrosion inhibitor during the early stage of copper corrosion under adsorbed thin electrolyte layers. *Corrosion Science*, 65, 214–222. DOI 10.1016/j.corsci.2012.08.019.
2. Huang, T. J., Yin, A. H., Liu, Z. Y. (2015). Setup of CO₂ corrosion simulation unit and test study under field site conditions in Jilin oilfield. *Surface Technology*, 3, 69–73.
3. Li, J. P., Zhao, G. X., Wang, Y. (2004). Static corrosion of oil thimble used in trim oil field. *Journal of Chinese Society for Corrosion and Protection*, 4, 24230–24233.
4. Geng, C. L., Gu, J., Xu, Y. M. (2011). Research progress on CO₂/H₂S corrosion and protection technique in oil and gas fields. *Material Review*, 25, 119–122.
5. Kermani, M. B., Morshed, A. (2003). Carbon dioxide corrosion in oil and gas production—a compendium. *Corrosion*, 59(8), 659–683. DOI 10.5006/1.3277596.
6. Islam, M. S., Otani, K., Sakairi, M. (2018). Effects of metal cations on mild steel corrosion in 10 mM Cl⁻ aqueous solution. *Corrosion Science*, 131, 17–27. DOI 10.1016/j.corsci.2017.11.015.
7. Otani, K., Islam, M. S., Sakairi, M. (2017). Inhibition ability of gluconates for fresh water corrosion of mild steel enhanced by metal cations. *Journal of the Electrochemical Society*, 164(9), C498–C504. DOI 10.1149/2.0491709jes.
8. Khedr, M. G. A., Lashien, A. M. S. (1992). Corrosion and corrosion inhibition of aluminium in aqueous solutions. *Corrosion Science*, 33(1), 137–151. DOI 10.1016/0010-938X(92)90023-V.
9. Otani, K., Sakairi, M. (2016). Effects of metal cations on corrosion of mild steel in model fresh water. *Corrosion Science*, 111, 302–312. DOI 10.1016/j.corsci.2016.05.020.
10. Goulart, C. M., Esteves-Souza, A., Martinez-Huitl, A. C. A., Rodrigues, C. J. F., Medeiros Maciel, M. A. et al. (2013). Experimental and theoretical evaluation of semicarbazones and thiosemicarbazones as organic corrosion inhibitors. *Corrosion Science*, 67, 281–291. DOI 10.1016/j.corsci.2012.10.029.
11. Solmaz, R. (2010). Investigation of the inhibition effect of 5-((E)-4-phenylbuta-1,3-dienylideneamino)-1,3,4-thiadiazole-2-thiol Schiff base on mild steel corrosion in hydrochloric acid. *Corrosion Science*, 52(10), 3321–3330. DOI 10.1016/j.corsci.2010.06.001.
12. Ech-chihbi, E., Belghiti, M. E., Salim, R., Oudda, H., Taleb, M. et al. (2019). Experimental and computational studies on the inhibition performance of the organic compound 2-phenylimidazo [1,2-a]pyrimidine-3-carbaldehyde against the corrosion of carbon steel in 1.0 M HCl solution. *Surface Interfaces*, 9, 206–217. DOI 10.1016/j.surfin.2017.09.012.
13. Han, J., Zhang, J., Carey, J. W. (2011). Effect of bicarbonate on corrosion of carbon steel in CO₂ saturated brines. *International Journal of Greenhouse Gas Control*, 5(6), 1680–1683. DOI 10.1016/j.ijggc.2011.08.003.
14. Zhang, G. A., Cheng, Y. F. (2009). On the fundamentals of electrochemical corrosion of X65 steel in CO₂-containing formation water in the presence of acetic acid in petroleum production. *Corrosion Science*, 51(1), 87–94. DOI 10.1016/j.corsci.2008.10.013.
15. Liu, H. W., Gu, T. Y., Zhang, G. A., Wang, W., Dong, S. et al. (2016). Corrosion inhibition of carbon steel in CO₂-containing oil field produced water in the presence of iron-oxidizing bacteria and inhibitors. *Corrosion Science*, 105, 149–160. DOI 10.1016/j.corsci.2016.01.012.
16. Ye, Y. W., Zou, Y. J., Jiang, Z. L., Yang, Q. M., Chen, L. Y. et al. (2020). An effective corrosion inhibitor of N doped carbon dots for Q235 steel in 1 M HCl solution. *Journal of Alloys and Compounds*, 815, 152338. DOI 10.1016/j.jallcom.2019.152338.
17. Wang, Y., Hu, J., Wang, Y. Q. (2016). A new method for preventing corrosion failure: thiourea and hexamethylenetetramine as inhibitor for copper. *Bulletin of the Korean Chemical Society*, 37(11), 1797–1811. DOI 10.1002/bkcs.10978.

18. Kaya, S., Guo, L., Kaya, C., Tüzün, B., Obot, I. B. et al. (2016). Quantum chemical and molecular dynamic simulation studies for the prediction of inhibition efficiencies of some piperidine derivatives on the corrosion of iron. *Journal of the Taiwan Institute of Chemical Engineers*, 65, 522–529. DOI 10.1016/j.jtice.2016.05.034.
19. Shahraki, M., Dehdab, M., Elmi, S. (2016). Theoretical studies on the corrosion inhibition performance of three amine derivatives on carbon steel: molecular dynamics simulation and density functional theory approaches. *Journal of the Taiwan Institute of Chemical Engineers*, 62, 313–321. DOI 10.1016/j.jtice.2016.02.010.
20. Xie, S. W., Liu, Z., Han, G. C., Li, W., Liu, J. et al. (2015). Molecular dynamics simulation of inhibition mechanism of 3,5-dibromo salicylaldehyde Schiff's base. *Computational and Theoretical Chemistry*, 1063, 50–62. DOI 10.1016/j.comptc.2015.04.003.
21. Hu, J., Chen, W., Zhao, X., Su, H. B., Chen, Z. (2018). Anisotropic electronic characteristics, adsorption, and stability of low-index BiVO₄ surfaces for photoelectrochemical applications. *ACS Applied Materials & Interfaces*, 10(6), 5475–5484. DOI 10.1021/acsami.7b15243.
22. Klamt, A., Schüürmann, G. (1993). COSMO: a new approach to dielectric screening in solvents with explicit expressions for the screening energy and its gradient. *Journal of the Chemical Society-Perkin Transactions*, 2 (5), 799–805. DOI 10.1039/P29930000799.
23. Deng, S. D., Du, G. B., Li, X. H., Pizzi, A. (2014). Performance and reaction mechanism of zero formaldehyde-emission urea-glyoxal (UG) resin. *Journal of the Taiwan Institute of Chemical Engineers*, 45(4), 2029–2038. DOI 10.1016/j.jtice.2014.02.007.
24. Wazzan, N. A., Obot, I. B., Kaya, S. (2016). Theoretical modeling and molecular level insights into the corrosion inhibition activity of 2-amino-1,3,4-thiadiazole and its 5-alkyl derivatives. *Journal of Molecular Liquids*, 221, 579–602. DOI 10.1016/j.molliq.2016.06.011.
25. Zhao, W., Wang, J. D., Liu, F. B., Chen, D. R. (2009). First principles study of H₂O molecule adsorption on Fe (100), Fe(110) and Fe(111) surfaces. *Acta Physica Sinica*, 58, 3352–3358.
26. Guo, L., Obot, I. B., Zheng, X., Shen, X., Qiang, Y. et al. (2017). Theoretical insight into an empirical rule about organic corrosion inhibitors containing nitrogen, oxygen, and sulfur atoms. *Applied Surface Science*, 406, 301–306. DOI 10.1016/j.apsusc.2017.02.134.
27. Liu, G., Chen, S., Ma, H. F., Liu, X. (2007). Molecular simulation study of 1,5-diphenylcarbazide self-assembled monolayers on a copper surface. *Journal of the Serbian Chemical Society*, 72(5), 475–484. DOI 10.2298/JSC0705475L.
28. Bahlakeh, G., Ramezanzadeh, B., Ramezanzadeh, M. (2019). The role of chrome and zinc free-based neodymium oxide nanofilm on adhesion and corrosion protection properties of polyester/melamine coating on mild steel: experimental and molecular dynamics simulation study. *Journal of Cleaner Production*, 210, 872–886. DOI 10.1016/j.jclepro.2018.11.089.
29. Yang, W., Lee, C., Ghosh, S. K. (1985). Theoretical studies on the corrosion inhibition performance of three amine derivatives on carbon steel: molecular dynamics simulation and density functional theory approaches. *Journal of Physical Chemistry C*, 89(25), 5412–5414. DOI 10.1021/j100271a019.
30. Hu, J., Wang, Z., Wang, T. T., Xu, P. Y., Li, N. (2019). Investigation on the synergy mechanism of mixed inhibitors—Mannich base and Na₂WO₄ on Fe surface by molecules dynamic simulation. *Molecular Simulation*, 45, 927–934.
31. Nosé, S. (1984). A unified formulation of the constant temperature molecular-dynamics methods. *Journal of Chemical Physics*, 81, 511–519.
32. Hoover, W. G. (1985). Canonical dynamics: equilibrium phase-space distributions. *Physical Review A*, 31(3), 1695–1697. DOI 10.1103/PhysRevA.31.1695.
33. Bazooyar, F., Momany, F. A., Bolton, K. (2012). Validating empirical force fields for molecular-level simulation of cellulose dissolution. *Computational and Theoretical Chemistry*, 984, 119–127. DOI 10.1016/j.comptc.2012.01.020.
34. Yang, W., Parr, R. G. (1985). Softness and the Fukui function in the electronic theory of metals and catalysis. *Proceedings of the National Academy of Sciences of the United States of America*, 82(20), 6723–6726. DOI 10.1073/pnas.82.20.6723.

35. Chattaraj, P. K., Sarkar, U., Roy, D. R. (2006). Electrophilicity index. *Chemical Reviews*, 106(6), 2065–2091. DOI 10.1021/cr040109f.
36. Hu, J., Chen, W., Zhao, X., Su, H. B., Chen, Z. (2018). Anisotropic electronic characteristics, adsorption, and stability of low-index BiVO₄ surfaces for photoelectrochemical applications. *ACS Applied Materials & Interfaces*, 10(6), 5475–5484. DOI 10.1021/acsami.7b15243.
37. Lou, Y. M., Liu, J. H., Zhou, X. P., Liu, J. C. (2009). Temperature on the viscosity and diffusion coefficient of water. *Southwest China Normal University (Natural Science Edition)*, 34, 34–39.
38. Zhang, X. Y., Kang, Q. X., Wang, Y. (2018). Theoretical study of N-thiazolyl-2-cyanoacetamide derivatives as corrosion inhibitor for aluminum in alkaline environments. *Computational and Theoretical Chemistry*, 1131, 25–32. DOI 10.1016/j.comptc.2018.03.026.
39. Guo, A. L., Duan, G. C., He, K., Sun, B. (2013). Synergistic effect between 2-oleyl-1-oleylamidoethyl imidazoline ammonium methylsulfate and halide ion by molecular dynamics simulation. *Computational and Theoretical Chemistry*, 1015, 21–26. DOI 10.1016/j.comptc.2013.04.001.
40. Hu, S. Q., Guo, A. L., Yan, Y. G., Jia, X. L. (2011). Computer simulation of diffusion of corrosive particle in corrosion inhibitor membrane. *Computational and Theoretical Chemistry*, 964, 176–181.
41. Chen, Y., Liu, Q. L., Zhu, A. M. (2010). Molecular simulation of CO₂/CH₄ permeabilities in polyamide-imide isomers. *Journal of Membrane Science*, 348, 204–212.
42. Zhang, L. S., Wang, Y. G., Wu, G. (2008). Study on the gas diffusion in olefin copolymer membrane by molecular dynamics simulation. *Revue Scientifique Et Technique-Office International Des Epizooties*, 26, 52–57.